ISSN (Online): 2456-5717

International Journal of Advanced Research in Basic Engineering Sciences and Technology (IJARBEST)
Vol.3 Issue.8 August 2017

Wingtip Vortex Alleviation Using a Reverse Delta Type Add-on Device

Afaq Altaf[1], Tan Boon Thong[2], Ashraf Ali Omar[3], Waqar Asrar[4]

[1]New York Institute of Technology Abu Dhabi, P.O. Box 5464, Abu Dhabi, United Arab Emirates.

[2]Monash University Malaysia, Selangor 47500, Malaysia.

[3]University of Tripoli, P.O. Box 81507, Tripoli, Libya.

[4]International Islamic University Malaysia, P.O. Box 10, Kuala Lumpur 50728, Malaysia.

Abstract:- The result of interactions of a wingtip vortex of a half-span wing and vortices generated by a slender reverse delta type add-on device were studied using Particle Image Velocimetry in a closed-loop low-speed wind tunnel. Characteristics of the vortex interactions produced downstream in planes perpendicular to the free stream direction at a mean chord-based Reynolds number, $Re_c = 2.75\times10^5$, are explored in this work. The study reveals that the reverse delta type add-on device considerably reduces the tangential velocity, vorticity and circulation magnitude of the resultant vortex by up to 79.6%, 85.6% and 48.7%, respectively. It was also found that the resultant vortex core radius increased by a factor of 5.63. Using a six component force balance, the reduction in lift and the increase in drag of the half-span wing with the reverse delta type add-on device was recorded to be 2.9% and 14.5%, respectively.

Keywords: Vortex, Reverse Delta Type Add-on Device, Particle Image Velocimetry (PIV)

NOMENCLATURE

C_D = drag coefficient

C_L = lift coefficient

C_m = pitching moment coefficient

b = wing span length (m)

k = number of points

L/D = lift to drag ratio

Re_c = Reynolds number based on chord length

r = radius, m

r_c = core radius, m

V_θ = tangential velocity, m/s

V_∞ = free stream velocity, m/s

x = stream-wise coordinate, m

y = span-wise coordinate, m

z = transverse coordinate, m

α = angle of attack, deg.

Γ = circulation, m^2/s

I. INTRODUCTION

Due to the continuous air traffic growth, present separation rules are becoming extremely insufficient to cope with future air traffic requirements. This study is driven with the objective of reducing the present air traffic spacing while sustaining the same level of safety.

Understanding of wake vortex behavior would lead to the development of constructive measures of control. The study and control of swirling vortex flows is vital towards developing ways to suppress wingtip and flap-tip vortices generated by commercial aircraft and result in their rapid decay which leads to a reduction in the hazard posed to trailing aircraft [1, 2].

All aircraft create wake vortices which are an unavoidable result of the creation of lift. Wake vortices are created by high pressure air from the lower surface of the wing flowing around the wingtip/flap-tip into the low pressure air above the wing. The result is a pair of vortices that originate from the wingtips/flap-tips in opposite directions, creating an area of turbulence behind the aircraft. The intensity of the wake vortices produced by a specific aircraft is determined by factors such as the aircraft's weight, speed, configuration (amount of flaps and slats extension), wingspan, angle of attack and the atmospheric conditions in which the aircraft is being flown [3]. Trailing vortices from wingtips have been observed to persist for many miles [4] and wake vortex encounters pose a serious threat to trailing aircraft, particularly when the trailing aircraft are smaller in size [5], that fly in close proximity near the airport runway during takeoff and landing [6] because the wake vortex circulation is at a maximum. A trailing aircraft's position and orientation with respect to the wake shed by a large lead aircraft is of major concern as the trailing aircraft may experience sudden upwash

or downwash, uncontrollable rolls and sudden loss of altitude [7].

Wake turbulence has resulted in fatal accidents at low altitudes during landing approaches because of inadequate time and altitude for pilots to recover full control of their aircraft after being violently affected by the strong vortices. Statistical data about wake turbulence indicates that more than half of wake turbulence accidents occur during approach and landing; most wake turbulence accidents occur at very low heights; 90% of wake turbulence accidents involve small aircraft; and in 99% of reported events, the effects of wake turbulence are abrupt and occur without any warning [3].

In order to avoid wake vortex encounters, the International Civil Aviation Organization (ICAO) has prescribed a minimum separation criterion between two aircraft during the approach, landing and take-off corridors [8]. The regulations include aircraft segregation by size, controlling flight paths during take-off and landing, and keeping a fixed separation between aircrafts based on the size of the lead aircraft. The current spacing rules in place are based on worst case scenarios and allow far more separation distance between aircraft than is really needed to avoid accidents [9]. However, the financial repercussions of these separation requirements are staggering [10].

There is a need to find means of increasing the dissipation rate of vortex wakes as they are very slow to dissipate naturally. Wake vortex alleviation deals with reducing the effects of wake vortex by reducing the circulation intensity or increasing the vortex core dimensions through wing modification (using winglets or wing fences) so that wake vortex decay is accelerated. Since it is impossible to inhibit aircraft wake vortices, ways of alleviating, destroying or at least minimizing their intensity in the shortest time/distance have to be considered.

The most favourable concepts of vortex dissipation involve modification of wings by means of winglets or wing fences attached to the lower surface of the wing which either produces countersign vorticity that reduces the intensity of the rolled up vortex or causes the vortex core dimension to be considerably enlarged, accelerating vortex dissipation [11].

Aircrafts with multiple flaps and cut-outs (gaps) between the flaps, initially produce multiple vortices, which quickly combine into one vortex for each wing. Multiple vortex pair systems have been studied to create weaker wakes [12, 13, 14]. The addition of a strong vortex pair counter-rotating to the basic tip vortices can lead to more diffused vortices whose strength is the sum of the co-rotating and counter-rotating vortices.

Many devices have been used to alter the vortex rollup process and to inject instability in the wake of the aircraft so that the resultant vortex is more enlarged and diffused. Examples include a spoiler mounted on the wingtip [15], splines mounted downstream of the wingtip [16], spoilers of delta type plan-form deployed in the area of the outboard flap [17], a tip-mounted slender half delta wing [18], a reverse delta type add-on device mounted at the wingtip [19] and flap-tip [20].

Several studies have been carried out with reverse delta type add-on devices and suggest that they can be used in vortex alleviation [17, 19, 20]. Reverse delta type add-on device vortices appear to instill counter-sign vorticity into the wingtip and flap-tip vortices and modify the vortex roll up process [19, 20]. The interaction of the vortices creates an enlarged and diffused resultant vortex which enhances wake vortex decay.

This study attempts to minimize the wake vortex hazard posed on trailing aircraft by using a reverse delta type add-on device. Particle Image Velocimetry (PIV) is used to study the characteristics of the reverse delta type add-on device and half-span model wingtip vortex interaction. This investigation is a continuation of the wake vortex alleviation studies previously carried out by the author using a reverse delta type add-on device [19, 20].

II. Experimental Setup

a) The Wind Tunnel

The experiments were performed in the 2.3 m (width) by 1.5 m (height) by 6.0 m (length) closed-loop low-speed wind tunnel at the International Islamic University Malaysia (IIUM). The wind tunnel has a free-stream turbulence intensity of less than 0.11%.

The PIV charge coupled device (CCD) camera was placed in the flow stream at an approximate distance of 3 wing mean chord lengths downstream of the measurement plane resulting in nominal disturbance to the upstream flow. Zhang [21] found the influence of a blunt object, placed in the wind tunnel, on the flow in the measurement plane to be less than 5% on the scattering of vortex centers and less than 2% on the maximum vorticity if the distance between the measurement plane and the blunt object exceeds 2 mean chords of the experimental model. For this study, the effect of the CCD camera on the flow is considered to be negligible as it is more than 2 mean chords away from the measurement plane.

b) The Model

A half-span wing model with slat extension 15º and flap extension 20º, shown in Figure 1, is used in this study along with two sets of reverse delta type add-on devices, shown in Figure

2. The reverse delta type add-on device is placed on the half-span wing model as shown in Figure 1. The reverse delta type add-on device has a thickness of 3 mm, sweep angle 69.4° and bevel angle of 20°, and is attached to the main wing by a 35 mm high adjustable mounting. The reverse delta type add-on device is to be extended and used only during take-off and landing. For the rest of the flight envelop, the add-on device is retracted and to be stowed in the wing.

The geometric size of the reverse delta type add-on devices [for simplicity; the subscript rdw (reverse delta wing) will be used] was selected based on the lift and drag penalties associated with them. Aerodynamic performance tests on various add-on device sizes revealed that an add-on device smaller than the small reverse delta type add-on device (S-rdw) gives rise to a large lift penalty and an add-on device larger than the large reverse delta type add-on device (L-rdw) gives rise to a large drag penalty. Therefore, S-rdw and L-rdw were selected because nominal lift and drag penalties were associated with them.

The location of the add-on device attachment on the main wing was selected based on the idea that a fast growing instability within the wingtip vortex is required so that the roll-up process of the wingtip vortex may be modified by the vortices produced by the reverse delta type add-on device.

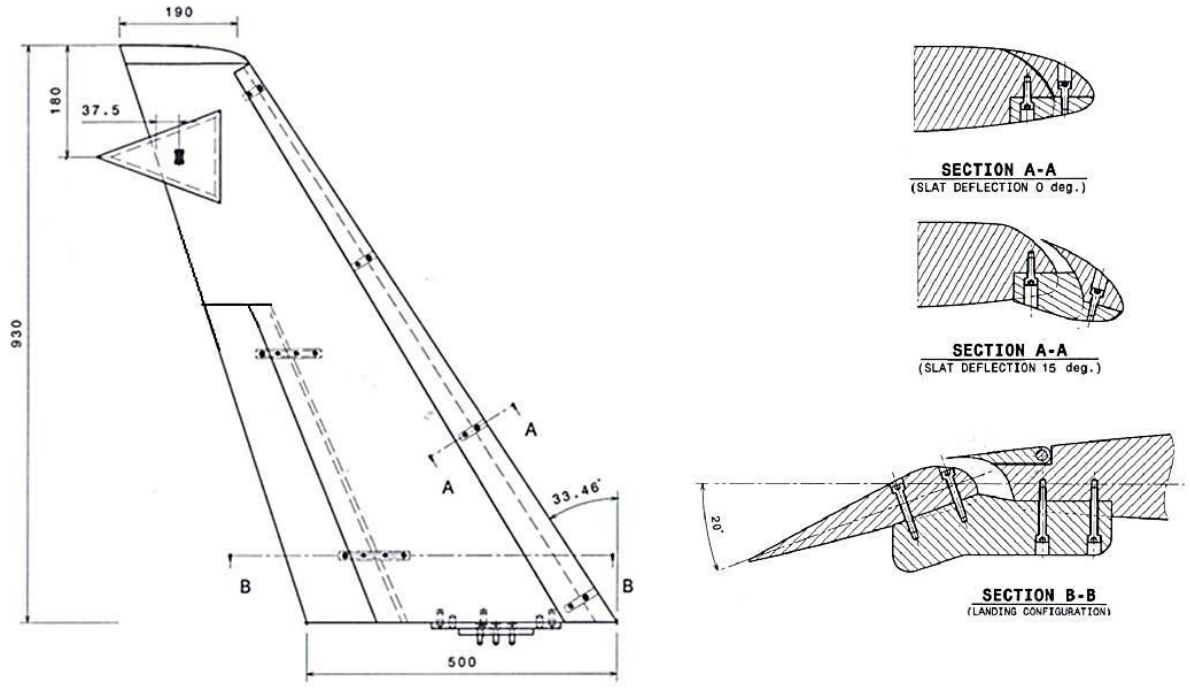

Figure 1: Schematic of the Wing model with a large reverse delta type add-on device (L-rdw) attached. Linear dimensions are in millimetres (mm).

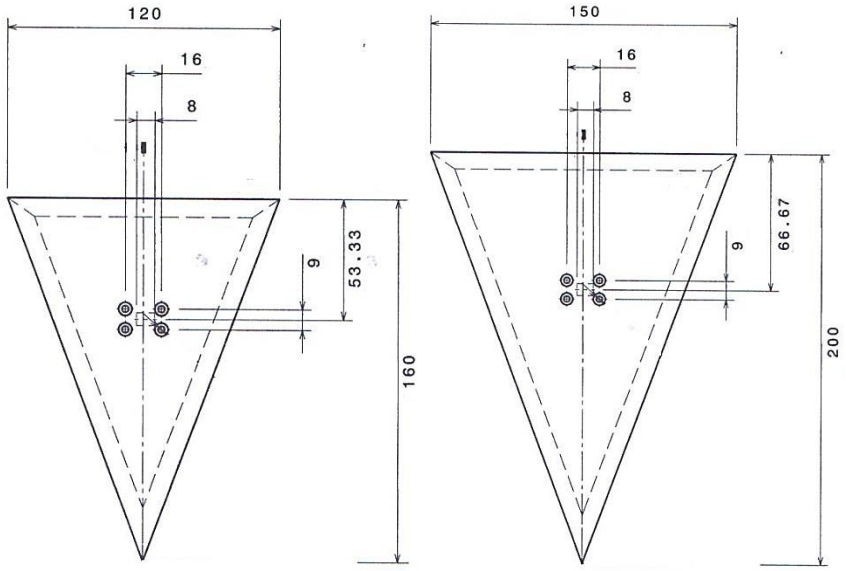

Figure 2: Schematic of the reverse delta type add-on devices (from left: small rdw add-on device (S-rdw) and large rdw add-on device (L-rdw)). Dimensions are in millimetres (mm).

c) Experimental Procedure

The velocity components in planes perpendicular to the stream-wise direction at four downstream locations are studied; $x/(b/2)$= 0.021, 0.548, 1.075 and 2.387. The stream-wise distance, x, is measured from the wingtip to the laser sheet position. The experimental setup is shown in Figure 3.

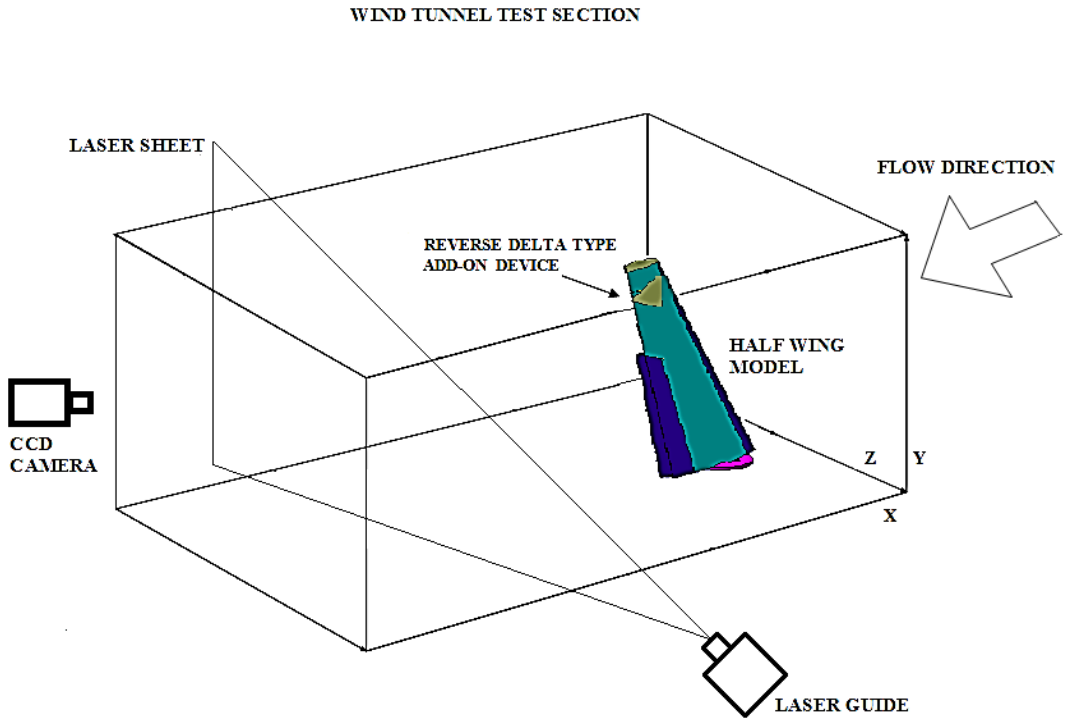

Figure 3: Schematic of the experimental setup.

The wind tunnel free stream velocity was set to 12 m/s corresponding to a mean chord-based Reynolds Number, $Re_c = 2.75 \times 10^5$. Seeding particles of a mean diameter of 1 μm were used and a light sheet from an Nd: YAG laser system of wavelength 532 nm was used to illuminate the flow. Laser sheet thickness of 2 mm was used. A CCD camera was placed perpendicular to the laser sheet, downstream of the half-span wing.

PIV data was obtained for the High Lift Configuration (HLC), slat extension 15º and flap extension 20º, at α=7.7º and HLC with reverse delta type add-on devices at α=9.7º. At 12 m/s and α=7.7º, the HLC yields a target lift coefficient C_L=1.06. For HLC with a reverse delta type add-on device, it was found that the target lift coefficient that was achieved at HLC without the add-on device is recovered when the half-span wing model angle of attack is increased by 2º. Therefore, the half-span wing model with the reverse delta type add-on device is tested at α=9.7º.

The add-on device angle of attack was fixed at α_{rdw}= +30º. Tests were also conducted for α_{rdw}= ±20° but the most favorable case of α_{rdw}= +30º, in terms of wake vortex alleviation, was chosen. 100 PIV images were recorded and post-processed using adaptive correlation with a 25% overlap for each case. The measurement resolution is 1600×1186 pixels. Initial interrogation area size of 256×256 pixels was reduced to a final interrogation area size of 32×32 pixels by making 3 refinement passes that yield 66×49 vectors per image. The 100 PIV vector maps were averaged to estimate the mean velocity in the region of focus.

III. RESULTS AND DISCUSSIONS

a) Velocity Vectors and Vorticity

Vortices are known to take several miles to dissipate downstream of a large aircraft. Vortex dissipation rate can be enhanced if the vortex core dimension is increased considerably by using vortex modification techniques such as using wing devices that can modify the vortex rollup process and introduce counter-sign vorticity into the vortex. A more dispersed vortex core at the same downstream position implies a weaker vortex [22].

The purpose of the half-span wing model – reverse delta type add-on device configuration, shown in Figure 1, is to investigate if the vortices shed by the reverse delta type add-on device will introduce a fast growing instability (counter-sign vorticity) into the wingtip vortex and alter the roll-up process of the wingtip vortex.

An uncertainty analysis of the PIV velocity measurements was performed using the International Organization for Standardization (ISO) procedure [23]. Based on 95% confidence intervals, the total uncertainty in the PIV velocity measurements was found to be ±0.19 m/s.

Figures 4 to 7 show the velocity vectors of a half-span wing model at HLC with/without a reverse delta type add-on device. The results are obtained at four downstream planes; x/ (b/2) = 0.021, 0.548, 1.075 and 2.387.

Figures 4a, 5a, 6a and 7a show the velocity vectors, tangential velocity magnitude and vorticity contours of the HLC wingtip vortex at the 4 downstream planes. Wingtip vortices are known to rollup extremely quickly [24]. It is noticeable that the wingtip vortex is nicely rolled up and is more compact at a farther downstream location. The reduction in tangential velocity magnitude between downstream planes is minimal, indicative of a strong vortex.

Figures 4b-c, 5b-c, 6b-c and 7b-c, show the velocity vectors, tangential velocity magnitude and vorticity contours of the vortices of the HLC with the add-on device in place. It is imperative to state that the tangential velocity magnitude is much lower at farther downstream planes when a reverse delta type add-on device is used. Reynolds [25] attributed the reduction in the tangential velocity to the increase in volume of the vortex in order to conserve momentum. The resultant vortex core size is seen to be increasing significantly between the downstream planes.

The wingtip vortex of the HLC without the add-on device exhibits a better rollup than the HLC with the add-on device, as shown in Figures 4a, 5a, 6a and 7a. The wingtip vortex tangential velocity magnitude is steady between downstream plane 1 and downstream plane 3. The wingtip vortex records a slight reduction in tangential velocity magnitude at downstream location 4. This suggests that the wingtip vortex is strong. At downstream plane 1, the add-on device cases exhibit higher tangential velocity magnitudes than the HLC case. This happens because the reverse delta type add-on device blocks the flow in its vicinity and the flow is forced to move around the reverse delta type add-on device. The flow moves along the span of the wing towards the wingtip and flap-tip. This accelerates the flow towards the wingtip and flap-tip, causing the existing flow at the wingtip and flap-tip to also accelerate. At farther downstream planes, the fluid physics are different as co-rotating and counter-rotating vortices (counter-sign vorticity exists), shed by the half-span model wingtip and the reverse delta type add-on device, exist and merge to form a weaker diffused resultant vortex. The tangential velocity reduction from downstream plane 1 to downstream plane 4 for

the HLC is 7.6% only. Whereas, the tangential velocity reduction between HLC and HLC with the add-on device at downstream plane 2 for the S-rdw case and L-rdw case is 7.7% and 20.6%, respectively. At downstream plane 3, the tangential velocity reduction between HLC and HLC with the add-on device for S-rdw and L-rdw cases is 30.9% and 57.0%, respectively. At downstream plane 4, the tangential velocity reduction between HLC and HLC with the add-on device for S-rdw and L-rdw cases is 54.3% and 79.6%, respectively.

The interaction of the wingtip vortex with the vortices generated by the add-on device yields a vortex with a weaker rollup which causes an increase in the vortex core size and also rejection of vorticity from the vortex core. The vortex system with co-rotating and counter-rotating vortices experiences a lower tangential velocity due to instabilities created by the interaction of the co-rotating and counter-rotating vortices within the vortex system which lead to an enlarged and diffused resultant vortex [1]. The wingtip vortex and the reverse delta type add-on device vortex in close proximity of the wingtip are co-rotating vortices. These co-rotating vortices are very close to each other and at the point where the vortices meet; they have opposite direction of rotation. This interaction lowers the tangential velocity of the resultant vortex and causes it to diffuse rapidly. It can be concluded that the introduction of a reverse delta type add-on device enhances the dissipation rate of the resultant vortex.

For all studied cases, the vorticity decreased steadily from a maximum at the center to nearly zero at the outer region of the vortices. From Figure 5a, it is seen that tiny patches of vorticity exist at the outer regions of the vortex, indicating that the entire vorticity shed by the half-span wing model is not deposited within the vortex core. From Figure 6a, it can be seen that the number of tiny patches of vorticity have reduced, indicating that more vorticity has been deposited within the vortex core. The vorticity magnitude at the center of the vortex in Figure 6a is marginally higher than in Figure 5a which supports the claim that more vorticity has diffused into the vortex core. In Figure 7a, the vorticity magnitude at the center of the vortex core has decreased and the tiny patches of vorticity have increased in number. This indicates that the vorticity from the vortex core may have been deposited in to the wake and hence, the vorticity magnitude decreases. The circulation and strength of the vortex are reduced due to the rejection of vorticity from the vortex core [26].

For the HLC with the add-on device, the vorticity is higher than the HLC case at downstream planes 1 and 2. This is because the tangential velocity magnitude of the resultant vortex at downstream plane 1 is higher. The vorticity reduces rapidly, as shown in Figures 4b-c, 5b-c, 6b-c and 7b-c. Distinguishable vortex contours within the vortex core can be seen.

The vortex core size is considerably larger than the HLC case. At downstream plane 4, the resultant vortex core (vorticity core) is mostly broken down and diffused, as shown in Figure 7b-c. The vorticity magnitude recorded is much lower than the HLC case. This highlights that there is rapid diffusion of vorticity from the vortex core in to regions outside the vortex core. The resultant vortex core has been significantly weakened and its strength has been reduced. The L-rdw case vortex exhibits lower vorticity magnitudes than the S-rdw case vortex at all four downstream planes. The larger the size of the add-on device, the stronger the counter-sign vorticity injected into the vortex system and the weaker the resultant vortex. The weak rolled up resultant vortex causes the vortex core size to increase significantly and also rejects vorticity in to regions outside the resultant vortex core. The weakened resultant vortex is seen to diffuse rapidly. The vorticity reduction from downstream plane 1 to downstream plane 4 for the HLC is 16.6% only. Since, the vorticity magnitudes at downstream planes 1 and 2 exhibited by the resultant vortex are higher than the HLC case, the reduction in vorticity can only be compared at downstream planes 3 and 4. The vorticity reduction between HLC and HLC with an add-on device at downstream plane 3 for the S-rdw case and L-rdw case is 42.3% and 74.9%, respectively. At downstream plane 4, the vorticity reduction between HLC and HLC with an add-on device for S-rdw case and L-rdw case is 59.0% and 85.6%, respectively.

The weaker vortices formed downstream of a wing with a reverse delta type add-on device are a desirable result. The weaker vortices will ensure that trailing aircrafts are not being engulfed in strong swirling flows during consecutive landings and take-offs. Thus, permitting for reduced separation of aircraft during landings and take-offs.

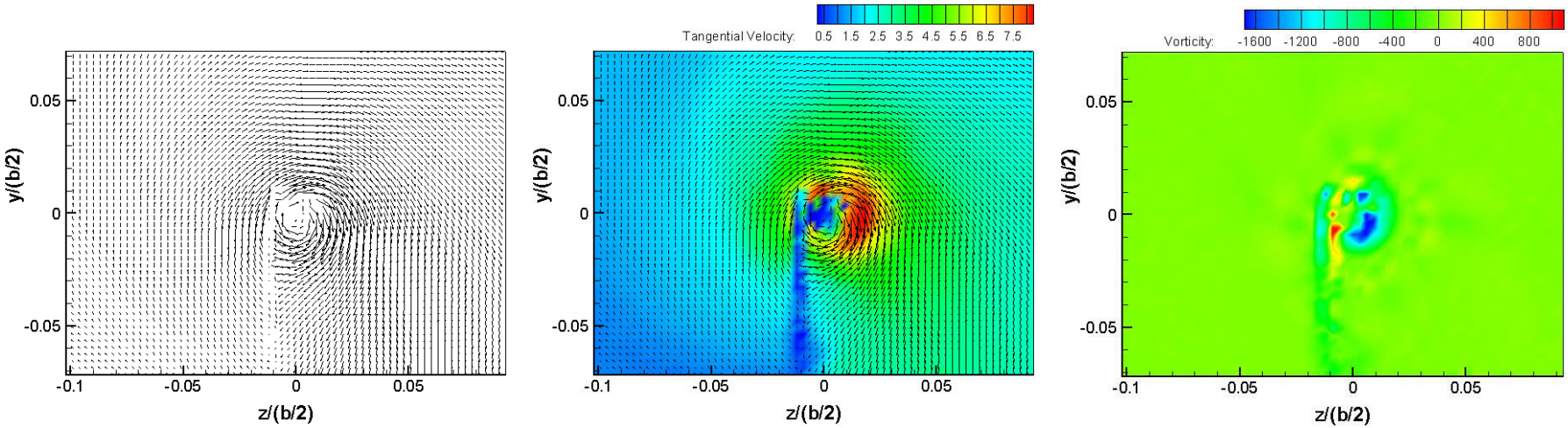

a) High Lift Configuration case, α=7.7º, x/(b/2)=0.021, V_∞=12 m/s.

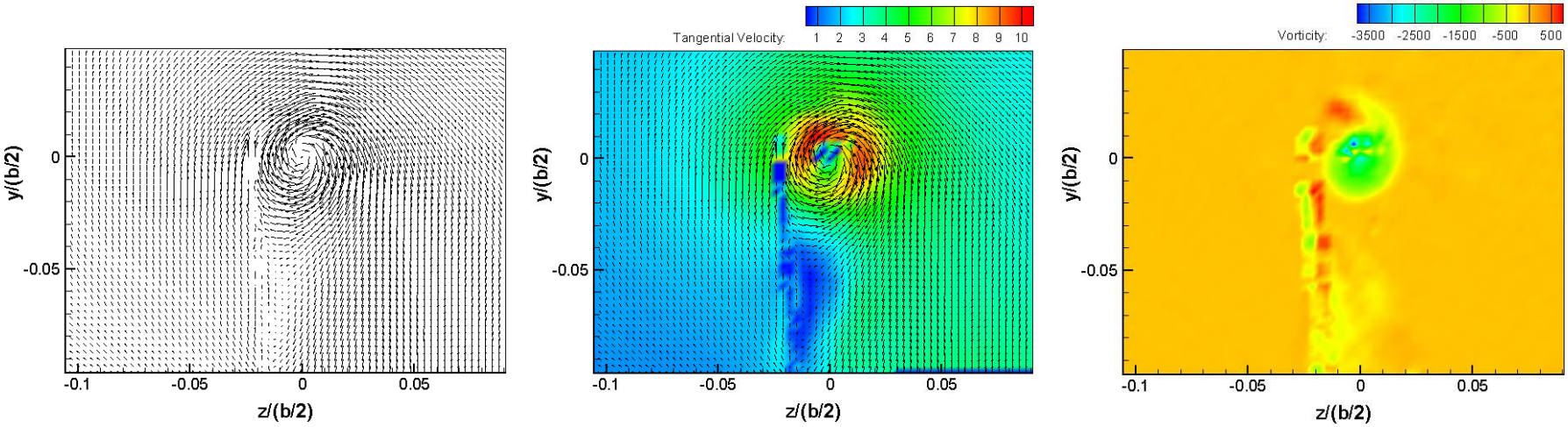

b) High Lift Configuration case, α=9.7º; with S-rdw add-on device, $\alpha_{S\text{-}rdw}$= +30º, x/(b/2)=0.021, V_∞=12 m/s.

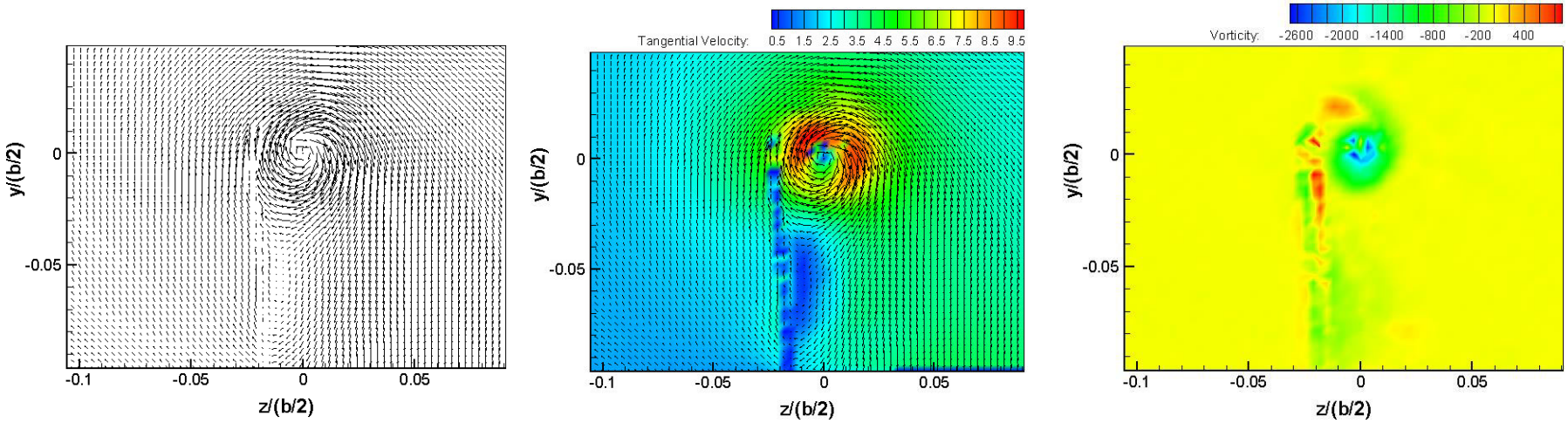

c) High Lift Configuration case, α=9.7º; with L-rdw add-on device, α_{Lrdw}= +30º, x/(b/2)=0.021, V_∞=12 m/s.

Figure 4: Velocity Vectors, Tangential Velocity Magnitude and Vorticity Contours at x/(b/2)=0.021 for (a) High Lift Configuration α=7.7º, (b) High Lift Configuration α=9.7º with S-rdw add-on device ($\alpha_{S\text{-}rdw}$= +30º) and (c) High Lift Configuration α=9.7º with L-rdw add-on device ($\alpha_{L\text{-}rdw}$= +30º).

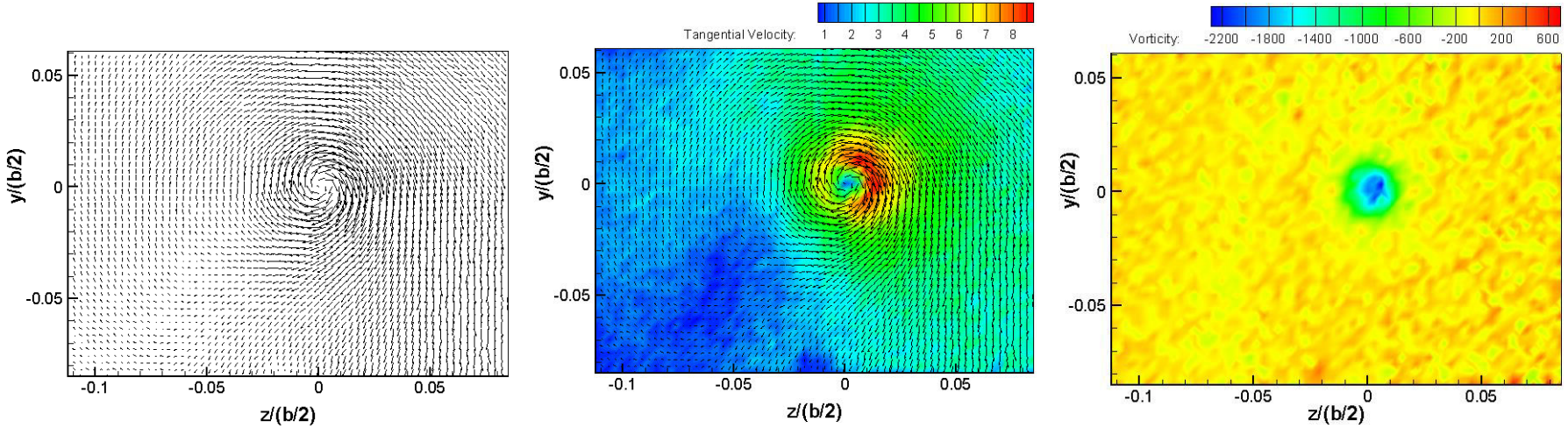

a) High Lift Configuration case, α=7.7º, x/(b/2)=0.548, V_∞=12 m/s.

ISSN (Online): 2456-5717

International Journal of Advanced Research in Basic Engineering Sciences and Technology (IJARBEST)
Vol.3 Issue.8 August 2017

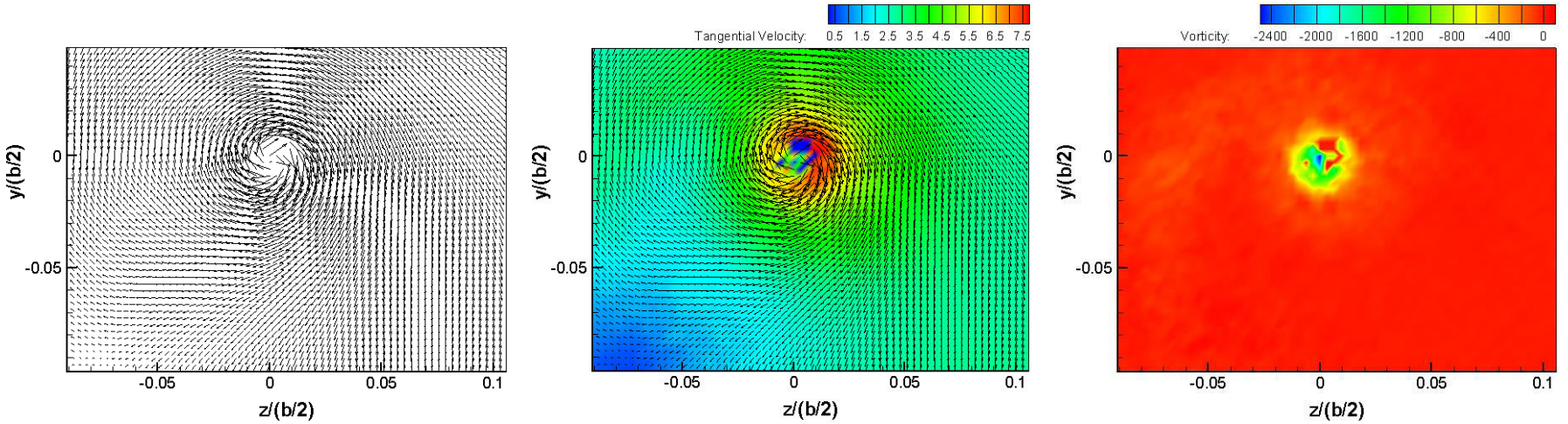

b) High Lift Configuration case, α=9.7º; with S-rdw add-on device, $\alpha_{S\text{-}rdw}$= +30º, x/(b/2)=0.548, V_∞=12 m/s.

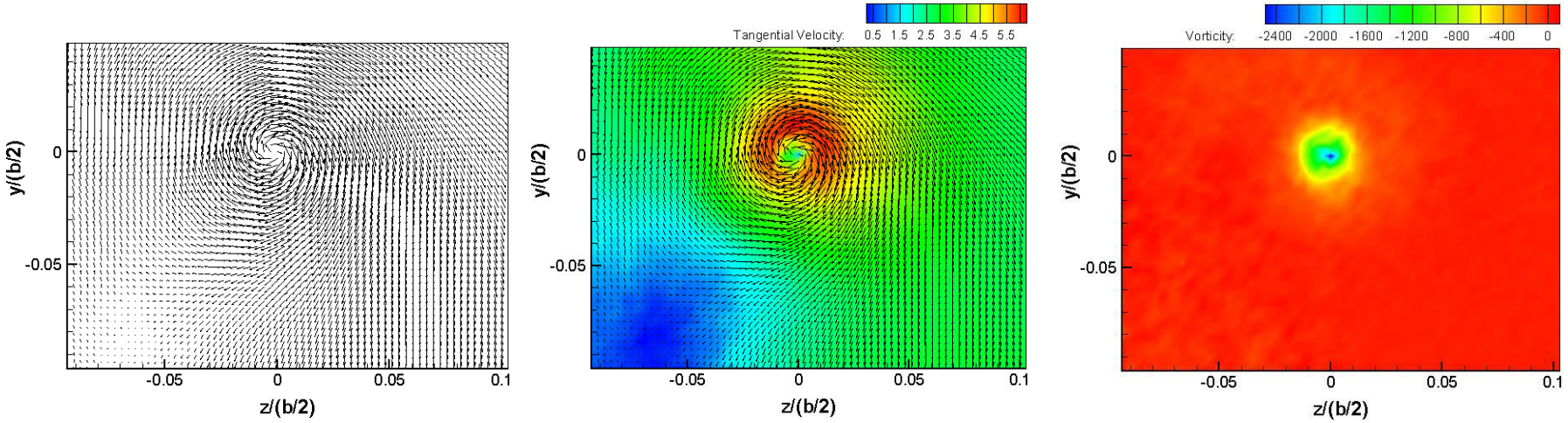

c) High Lift Configuration case, α=9.7º; with L-rdw add-on device, α_{Lrdw}= +30º, x/(b/2)=0.548, V_∞=12 m/s.

Figure 5: Velocity Vectors, Tangential Velocity Magnitude and Vorticity Contours at x/(b/2)=0.548 for (a) High Lift Configuration α=7.7º, (b) High Lift Configuration α=9.7º with S-rdw add-on device ($\alpha_{S\text{-}rdw}$= +30º) and (c) High Lift Configuration α=9.7º with L-rdw add-on device ($\alpha_{L\text{-}rdw}$= +30º).

ISSN (Online): 2456-5717

International Journal of Advanced Research in Basic Engineering Sciences and Technology (IJARBEST)
Vol.3 Issue.8 August 2017

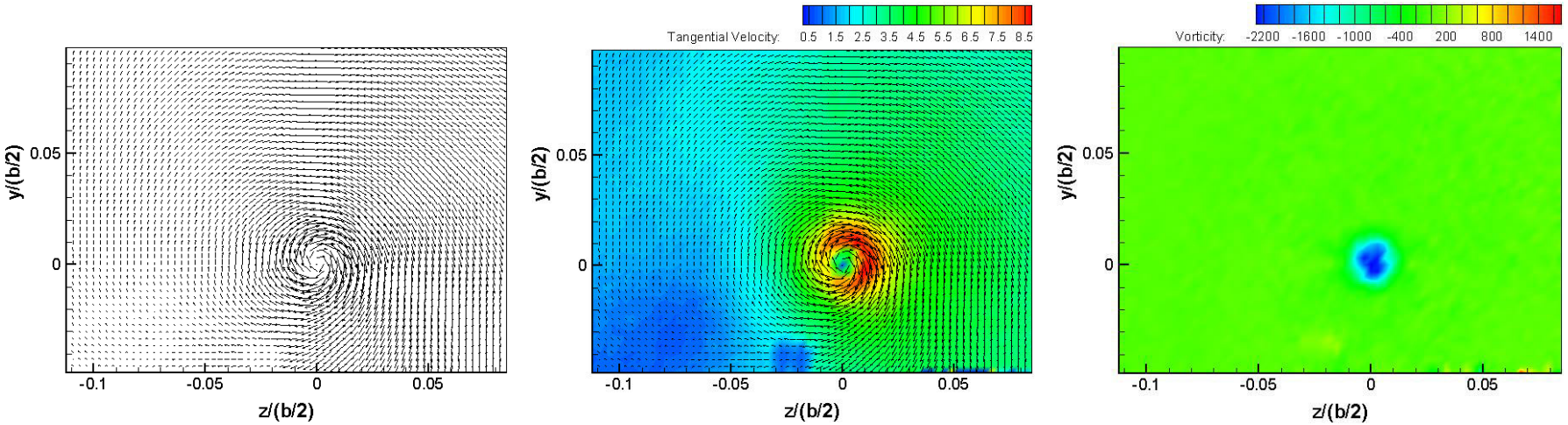

a) High Lift Configuration case, α=7.7º, x/c=1.075, V_∞=12 m/s.

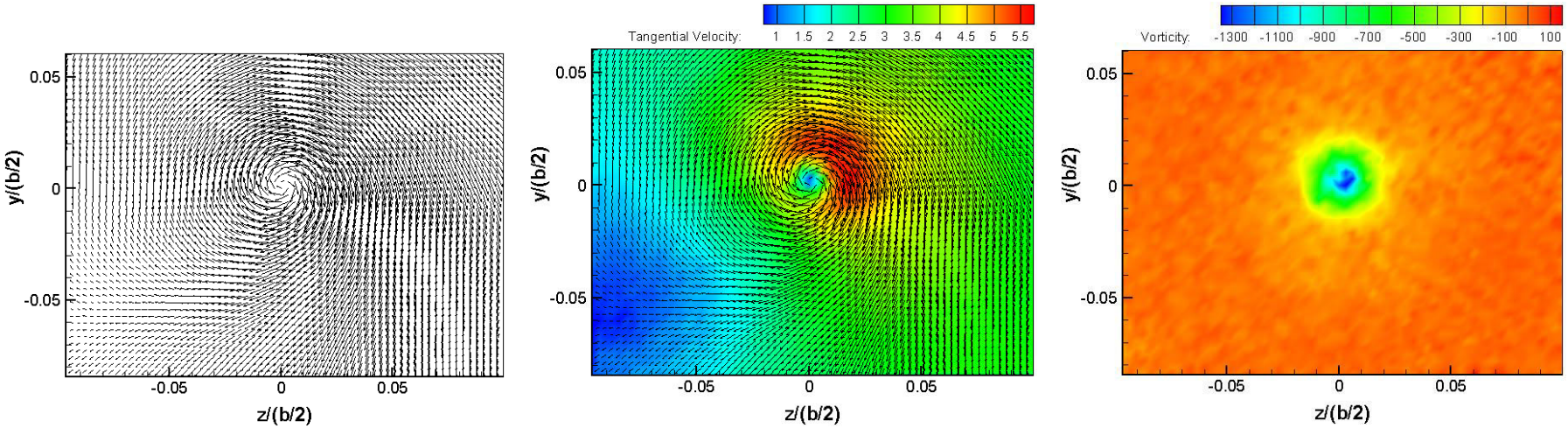

b) High Lift Configuration case, α=9.7º; with S-rdw add-on device, $\alpha_{S\text{-}rdw}$= +30º, x/(b/2)=1.075, V_∞=12 m/s.

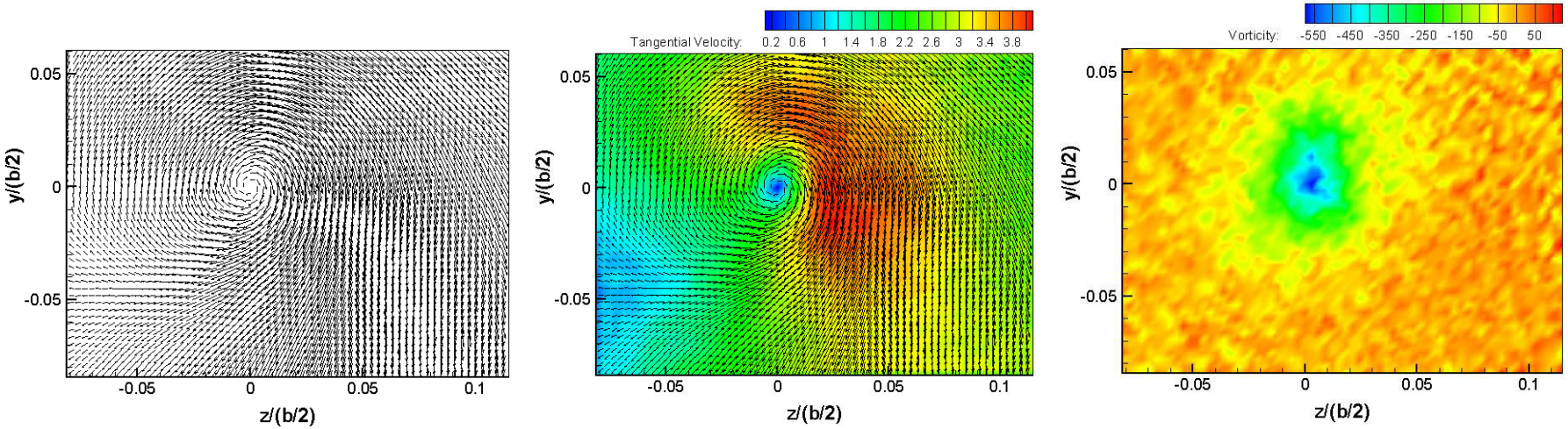

c) High Lift Configuration case, α=9.7º; with L-rdw add-on device, $\alpha_{L\text{-}rdw}$= +30º, x/(b/2)=1.075, V_∞=12 m/s.

Figure 6: Velocity Vectors, Tangential Velocity Magnitude and Vorticity Contours at x/(b/2)=1.075 for (a) High Lift Configuration α=7.7º, (b) High Lift Configuration α=9.7º with S-rdw add-on device ($\alpha_{S\text{-}rdw}$= +30º) and (c) High Lift Configuration α=9.7º with L-rdw add-on device ($\alpha_{L\text{-}rdw}$= +30º).

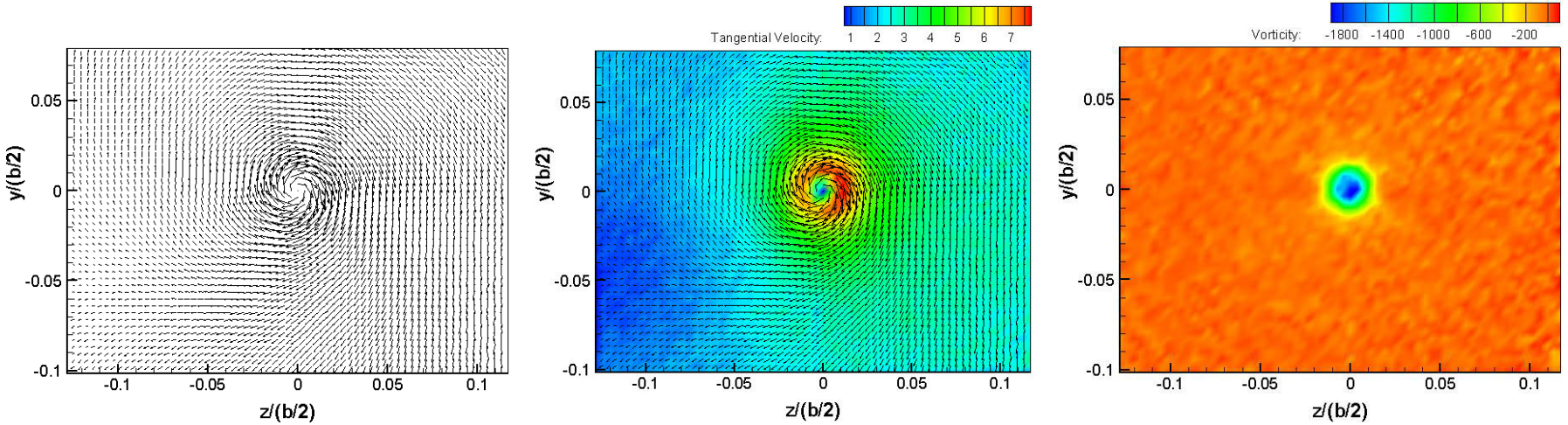

a) High Lift Configuration case, α=7.7º, x/c=2.387, V_∞=12 m/s.

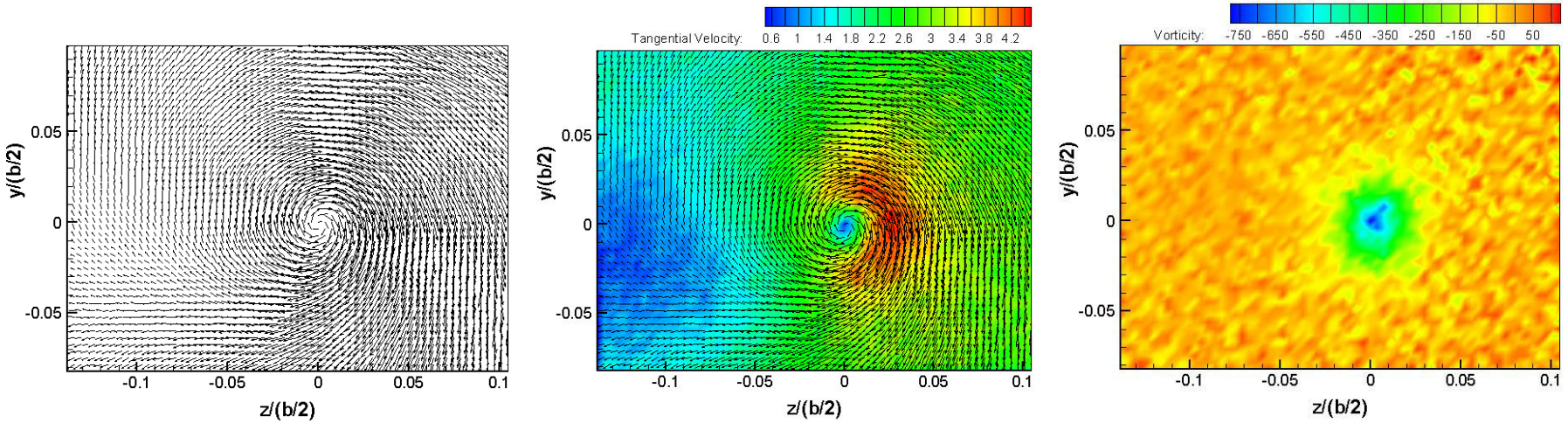

b) High Lift Configuration case, α=9.7º; with S-rdw add-on device, $\alpha_{S\text{-}rdw}$= +30º, x/(b/2)=2.387, V_∞=12 m/s.

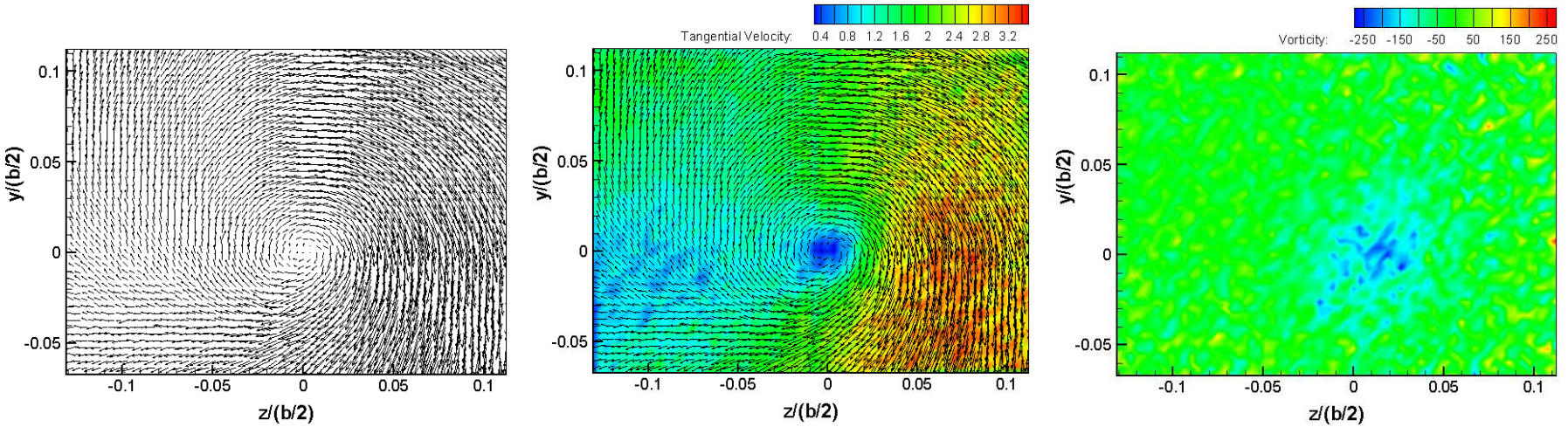

c) High Lift Configuration case, α=9.7º; with L-rdw add-on device, $\alpha_{L\text{-}rdw}$= +30º, x/(b/2)=2.387, V_∞=12 m/s.

Figure 7: Velocity Vectors, Tangential Velocity Magnitude and Vorticity Contours at x/(b/2)=2.387 for (a) High Lift Configuration α=7.7º, (b) High Lift Configuration α=9.7º with S-rdw add-on device ($\alpha_{S\text{-}rdw}$= +30º) and (c) High Lift Configuration α=9.7º with L-rdw add-on device ($\alpha_{L\text{-}rdw}$= +30º).

b) Tangential Velocity Distributions

The tangential velocity around the vortex centerline, V_θ, is calculated as

$$v_\theta(r) = \frac{1}{k}\sum_{i=1}^{k} v_{\theta,i}(y,z)\big|_{r=\sqrt{y^2+z^2}} \tag{1}$$

where k is the number of points for each radius; $r = \sqrt{y^2 + z^2}$. For this study, V_θ is normalized by the free stream velocity V_∞ and plotted versus the radial distance from the vortex centerline r, normalized by the half span (b/2); and r_c is defined as the vortex core radius, where maximum tangential velocity occurs [27].

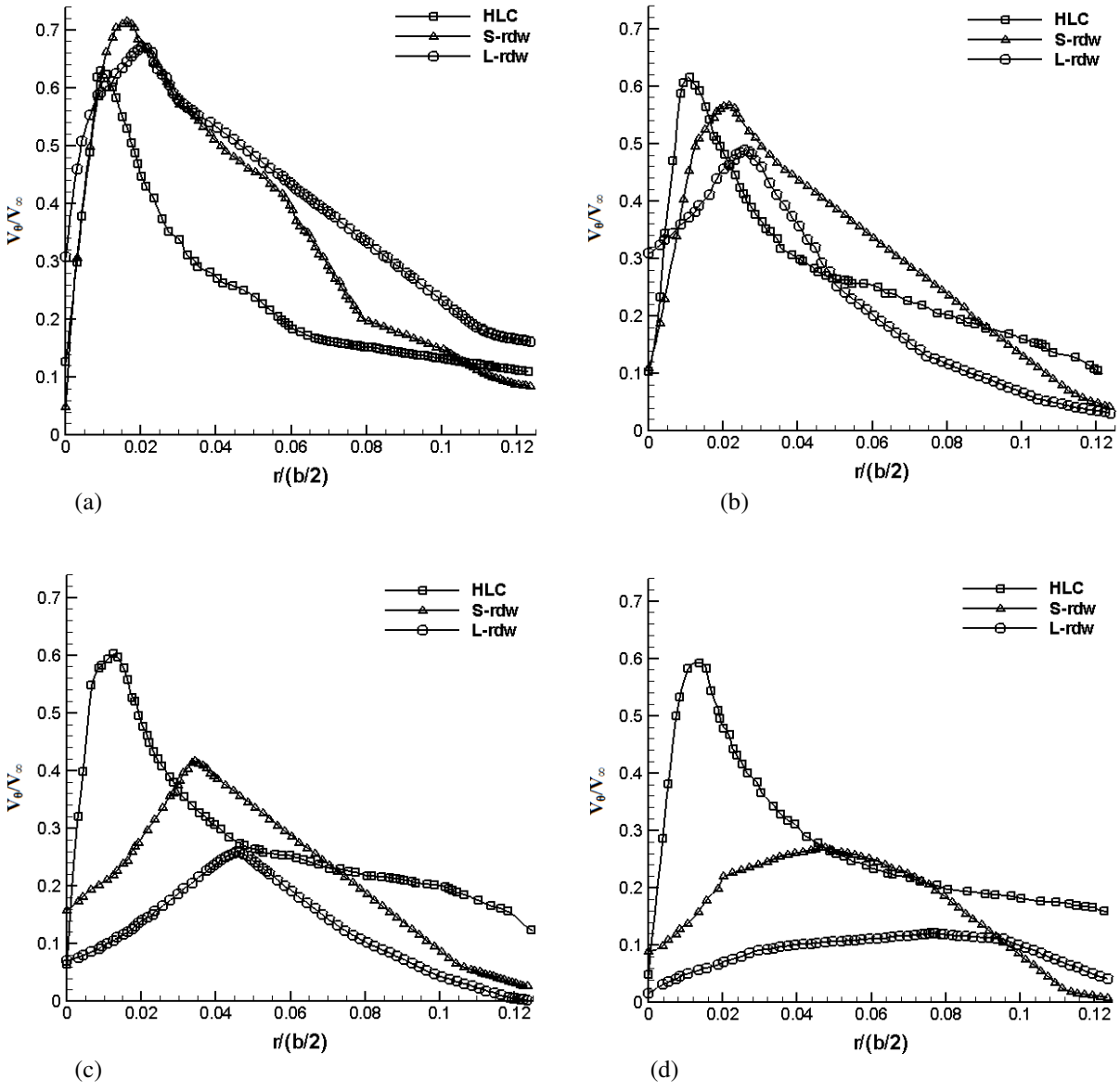

Figure 8: Non-dimensional tangential velocity distributions of HLC, HLC with S-rdw and HLC with L-rdw at (a) x/(b/2)=0.021, (b) x/(b/2)=0.548, (c) x/(b/2)=1.075 and (d) x/(b/2)=2.387.

The tangential velocity distributions of HLC, HLC with S-rdw and HLC with L-rdw at

downstream planes x/(b/2)= 0.021, 0.548, 1.075 and 2.387 are shown in Figures 8a-8d. The tangential velocity distributions increase rapidly to a maximum at the core radius, and then vary inversely. Figure 8a shows that the tangential velocity magnitude for the HLC case is lower than the tangential velocity magnitude for the add-on device cases. This is in agreement with Figures 4a-4c. From Figures 8b-8d, the HLC case without the add-on devices exhibits higher tangential velocity magnitude than the HLC case with the add-on devices. This is in agreement with Figures 4 to 7 for the HLC without the add-on devices. At a farther downstream location, the tangential velocity magnitude decreases for all studied cases due to vortex dissipation. The tangential velocity magnitude for the HLC with the add-on device cases decreases rapidly from downstream plane 2 to 4.

The HLC vortex core radius is much smaller compared to the HLC with the add-on device resultant vortex core radius at all four downstream locations. The difference in the sizes of the vortex cores is evident from the tangential velocity distributions. At x/(b/2)=0.021, the resultant vortex core radius (when add-on device is used) compared to the HLC vortex core radius has enlarged (diffused) by a factor of 1.72 and 2.23 for the S-rdw and L-rdw cases, respectively. At x/(b/2)=0.548, the resultant vortex core radius has increased by a factor of 1.93 and 2.31 for the S-rdw and L-rdw cases, respectively. At x/(b/2)=1.075, the resultant vortex core radius has increased by a factor of 2.72 and 3.62 for the S-rdw and L-rdw cases, respectively. At x/(b/2)=2.387, the resultant vortex core radius has increased by a factor of 3.39 and 5.63 for the S-rdw and L-rdw cases, respectively. This implies that when the L-rdw is used, the resultant core radius size is 5.63 times larger than the core radius of the HLC case. For HLC with S-rdw, the growth rate of the resultant vortex from plane 1 to 2 is 31.3%, from plane 2 to 3 is 61.9% and from plane 3 to 4 is 35.3%. For HLC with L-rdw, the growth rate of the resultant vortex from plane 1 to 2 is 21.7%, from plane 2 to 3 is 79.4% and from plane 3 to 4 is 69.2%. This indicates that the growth rate of the resultant vortex is greater than that of the wingtip vortex. This highlights the enormity of the diffusion of the resultant vortex caused when a reverse delta type add-on device is used. The enlarged resultant vortex is much weaker in strength and is expected to dissipate more rapidly than the HLC wingtip vortex.

c) Circulation Distributions

In Anderson [28] and Dobrev et al. [29], circulation is estimated by

$$\Gamma = \int_A \zeta \, dA \tag{2}$$

which in turn yields

$$\Gamma = 2\pi r v_\theta \tag{3}$$

for an axisymmetric vortex that is treated as a cylinder. For this study, the circulation is normalized by $V_\infty(b/2)$.

The circulation distributions for the HLC, HLC with S-rdw and HLC with L-rdw at downstream planes x/(b/2)= 0.021, 0.548, 1.075 and 2.387 are shown in Figures 9a to 9d. Between downstream plane 1 and 3, the circulation magnitude of the HLC case increases considerably. The circulation magnitude of the HLC vortex between downstream plane 3 and 4 is almost steady, indicating that the vortex strength has not reduced yet. The HLC vortex is still compact at downstream plane 4 and has not started to diffuse yet. The strength of the wingtip vortex will continue to increase until a maximum and then gradually decrease as the vortex starts to decay.

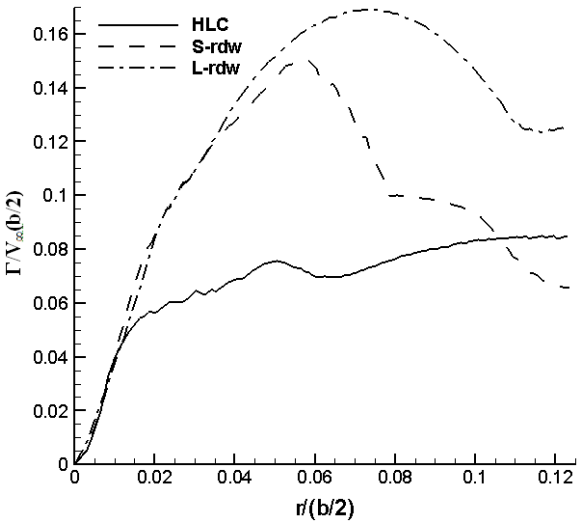

(a)

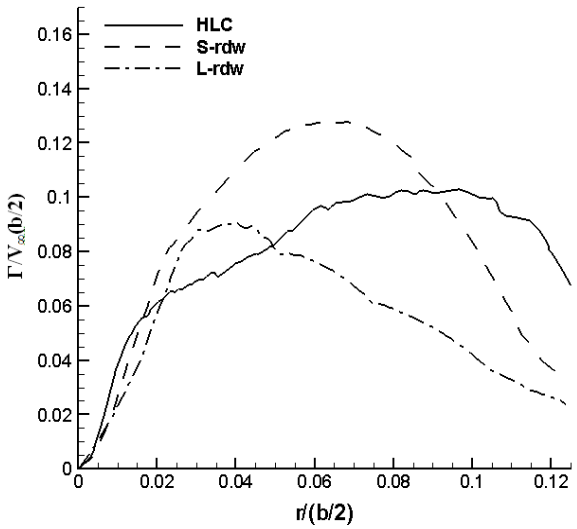

(b)

ISSN (Online): 2456-5717

International Journal of Advanced Research in Basic Engineering Sciences and Technology (IJARBEST)
Vol.3 Issue.8 August 2017

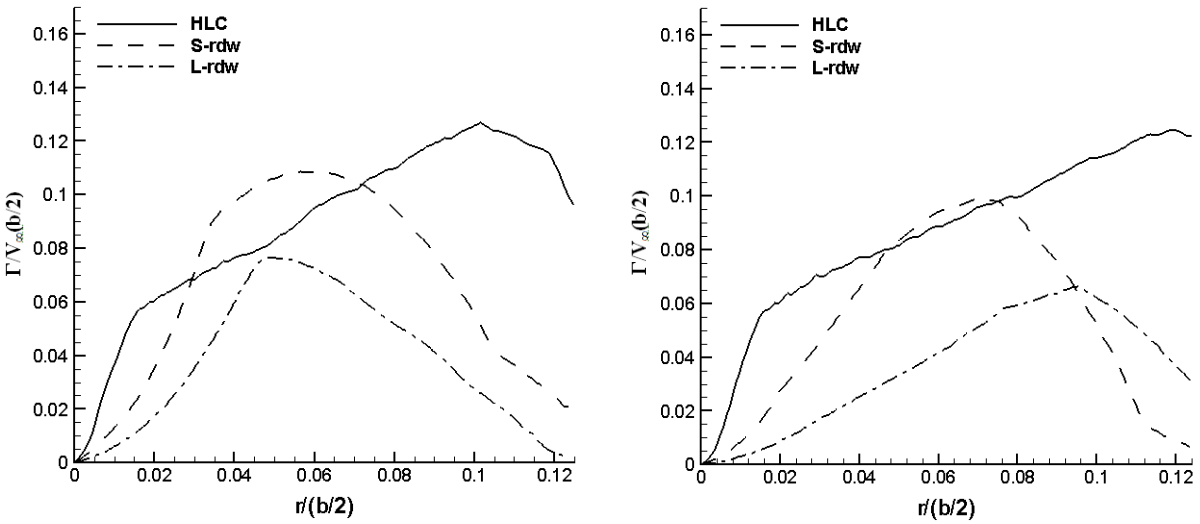

Figure 9: Vortex strength $\Gamma/V_\infty(b/2)$ versus radius r/(b/2) of wingtip vortex of HLC, HLC with S-rdw and HLC with L-rdw at (a) x/(b/2)=0.021, (b) x/(b/2)=0.548, (c) x/(b/2)=1.075 and (d) x/(b/2)=2.387.

The HLC with the reverse delta type add-on device shows that the circulation of the resultant vortex decreases steadily from downstream plane 1 to 4. At downstream planes 1 and 2, the circulation magnitude of the resultant vortex is higher than the HLC vortex because the tangential velocity and vorticity magnitudes are higher, as shown in Figures 9a and 9b. For the S-rdw and L-rdw cases, the circulation magnitude decreases significantly as counter-sign vorticity is injected in to the wingtip vortex by the add-on device. This weakens the resultant vortex and breaks down the resultant vortex core (vorticity core is broken down). Tiny individual vorticity patches are formed which have lower vorticity magnitudes. The decrease of vorticity magnitude in the resultant vortex core causes a decrease in its circulation (strength). At x/(b/2)= 1.075, the circulation magnitude for S-rdw case and L-rdw case has decreased by 14.4% and 39.6%, respectively. At x/(b/2)= 2.387, the circulation magnitude of the S-rdw case and L-rdw case has further decreased by 20.6% and 48.7%, respectively. There is significant decrease in the circulation magnitude from downstream plane 1 to 4 for the S-rdw and L-rdw cases and thus, it can be said that for these cases significant vortex decay has taken place as the resultant vortex core (vorticity core) has started to deform and is broken into many tiny vorticity patches (Figure 6c). It is expected that farther downstream, the circulation magnitude will continue to decrease and eventually become insignificant. From the circulation distributions trend, the L-rdw case resultant vortex is likely to decay more rapidly, followed by the S-rdw and HLC cases, respectively.

It can be concluded that the reverse delta type add-on device is capable of alleviating wake vortex significantly. From figures 9a-d, it can be concluded that the enlarged resultant vortex is weaker in strength and is expected to dissipate more rapidly than the HLC wingtip vortex.

d) Aerodynamic Performance

A six-component force balance was used to acquire the aerodynamic performance of the half-span wing model with/without the reverse delta type add-on device. The aerodynamic performance of the plain wing configuration (slat extension 0° and flap extension 0°) was also obtained. The add-on device angle of attack was fixed to α= +30° for all cases.

The lift coefficient (C_L) and moment coefficient (C_m) curves of all the studied cases are shown in Figure 10a. The HLC exhibits the highest lift coefficient at α=18°, and it stalls between α=18° and α=19°. The S-rdw and L-rdw configurations stall between α=19° and α=20°. This indicates that by using an add-on device the wing stall can be delayed by approximately 1°. This occurs because the air between the add-on device and the main wing is accelerated and hence, delays the flow separation over the main wing. The lift coefficient curves are almost identical until α=0° and then diverge slowly beyond that. The reduction in the lift coefficient values between the HLC, S-rdw and L-rdw cases is 2.9%. The moment coefficient curves show that the stability of the wing is maintained for all cases.

Figure 10b shows the drag coefficient (C_D) curves for all the cases. The drag increment (compared with the HLC drag as the base value at target lift coefficient) for S-rdw case is 6.9% and for L-rdw case is 14.5%. It was found that to maintain the target lift coefficient, an increase of 1.0° in the angle of attack of the half-span wing model is necessary to compensate for the reduction of lift when the add-on device is used. The increase of 1.0° in angle of attack of the half-span wing causes a 5.5% increase in drag. The findings of the study are listed in Table 1.

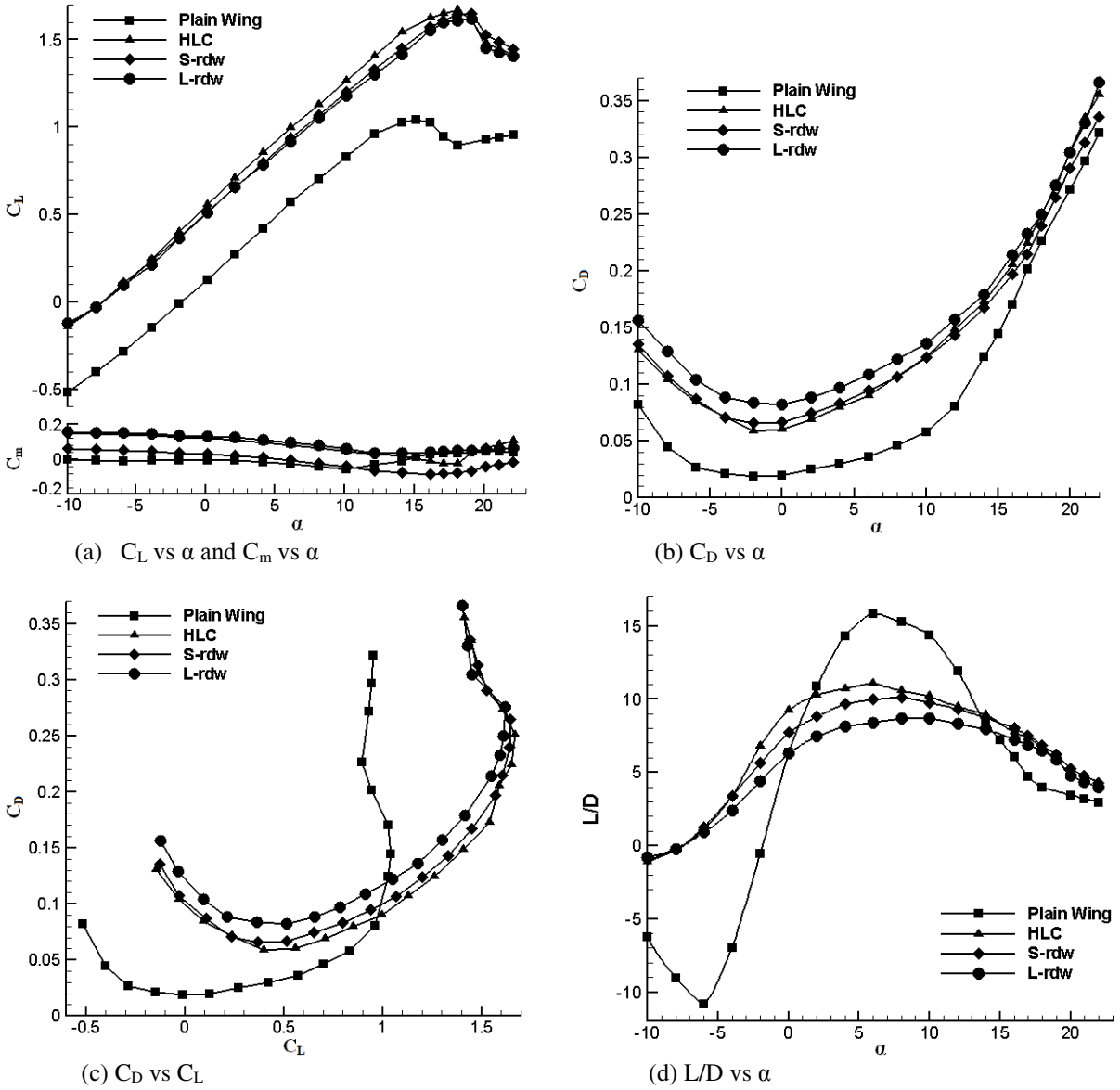

(a) C_L vs α and C_m vs α

(b) C_D vs α

(c) C_D vs C_L

(d) L/D vs α

Figure 10: Aerodynamic performance of the Plain Wing, HLC, HLC with S-rdw and HLC with L-rdw.

TABLE I: OVERALL FINDINGS OF THE INVESTIGATION

Vortex Core Size	Tangential Velocity	Vorticity	Circulation	Lift Coefficient	Drag Coefficient
+463% (factor of 5.63)	-79.6%	-85.6%	-48.7%	-2.9%	+14.5%

'+' indicates increase '-' indicates decrease

e) Comparison of lift and drag penalties with other techniques

TABLE II: COMPARISON OF LIFT AND DRAG PENALTIES WITH OTHER WAKE VORTEX ALLEVIATION TECHNIQUES

Authors	Device	Lift Reduction	Drag Increment
V. J. Rossow, 1978 [30]	Fins	No lift penalty	10%
D. R. Croom & G. T. Holbrook, 1979 [31]	Fins	13.3%	28.6%
E. Ozger, I. Schell & D. Jacob, 2001 [32]	Wing control surfaces and fins	7.0%	unavailable
Breitsamter, 2011 [17]	Double delta spoiler	2.9%	unavailable
Present Study	Reverse delta type add-on device	2.9%	14.5%

Table 2 provides a comparison of lift and drag penalties of the present study with other well-known wake vortex alleviation investigations. It can be seen from Table 2 that only Rossow's [30] investigation yields a lower increment in drag than the study of the reverse delta type add-on device. However, the benefits of the present study in terms of wake vortex alleviation are more superior to Rossow's study.

IV. CONCLUSION

Resultant vortex structures downstream of a half-span wing model at High Lift Configuration (HLC) with a reverse delta type add-on device were studied using Particle Image Velocimetry (PIV). A six component force balance was used to obtain the aerodynamic performance of the half-span wing model at four configurations.

The vortex structures showed that there was considerable reduction in tangential velocity, vorticity and circulation when the reverse delta type add-on devices were in use. The L-rdw case is more favourable as it gives rise to greater reduction in tangential velocity, vorticity and circulation magnitudes than the S-rdw case and the HLC case.

Between downstream planes 1 and 4, the maximum tangential velocity reduction recorded for the HLC case was 7.6% only whereas the maximum tangential velocity reduction for the S-rdw case and the L-rdw case compared to the HLC case was 54.3% and 79.6%, respectively; the maximum vorticity reduction recorded for HLC case was 16.6% only whereas the maximum vorticity reduction for the S-rdw case and the L-rdw case compared to the HLC case was 59.0% and 85.6%, respectively; the maximum circulation reduction recorded for the S-rdw case and the L-rdw case compared to the HLC case was 20.6% and

48.7%, respectively; the resultant vortex core radius compared to the HLC case increased by a factor of 3.39 and 5.63 for the S-rdw case and L-rdw case, respectively.

The above observations highlight several benefits of using a reverse delta type add-on device for wake vortex alleviation. The reverse delta type add-on device ensures that the resultant vortex strength is significantly weakened. The weak resultant vortex will continue to decay rapidly and safeguard trailing aircrafts from encountering hazardous vortical flows. This will allow aircraft spacing to be reduced, time between consecutive landings and take-offs to be reduced and aircraft capacity at airports to be increased.

The aerodynamic performance of the half-span wing model was moderately adversely affected by the use of a reverse delta type add-on device. The reduction in lift was 2.9% and the increase in drag was 14.5%.

More extensive research is required to expose the maximum potential of a reverse delta type add-on device has and it's capability to successfully alleviate the wake vortex hazard. Practical considerations will also need to be considered when implementing on actual aircraft. Issues that need to be addressed are stated as follows: A study of the extension of the add-on device (using actuators) in flight or in the wind tunnel with wind on condition should be studied to note the immediate effect on the change in aerodynamic performance of the wing; High accuracy experimental and computational investigations of the far wakes of aircraft with a reverse delta type add-on device are necessary to determine exactly how much spacing rules can be modified with no compromise in the level of safety; The effect of the mounting height of the reverse delta type add-on device should be studied extensively as it could have a great impact on the half-span wing model aerodynamics and flow characteristics; A reverse delta type add-on device at a combination of roll and pitch angles should be tested on a multi-element wing model in the wind tunnel.

ACKNOWLEDGEMENT

The author would like to thank International Islamic University Malaysia for permitting to conduct the experimental work at their closed-loop low-speed wind tunnel facility.

REFERENCES

[1] Coustols, E., Jacquin, L. and Shrauf, G. "Status of Wake Vortex Alleviation in the Frame Work of European Collaboration: Validation Attempts Using Tests and CFD Results." *ECCOMAS CFD conference*, Technical University of Delft, The Netherlands, 2006, pp. 1-20.

[2] Coustols, E. "An Overview of European Projects on Wake Vortices." *Proceedings of the Workshop on "Principles of Wake Vortex Alleviation Devices."* ONERA–The French Aerospace Lab, Toulouse, France, Feb. 2005.

[3] Veillette, P. R. "Data show that U.S. Wake-Turbulence Accidents are most frequent at Low Altitude and During Approach and Landing." *Flight Safety Foundation, Flight Safety Digest,* March – April 2002, pp. 1-56.

[4] Andrews, W. H. "Flight Evaluation of the Wing Vortex Wake Generated by Large Jet Transport." *Symposium on Aircraft Wake Turbulence,* Seattle, 1970.

[5] McGowen, W. A. "Trailing Vortex Hazard." *Society of Automotive Engineers Business Aircraft Meeting*, Wichita, Kansas, 1968.

[6] Arndt, R.E.A., Arakeri, V.H. and Higuchi, H. "Some Observations of Tip Vortex Cavitation." *Journal of Fluid Mechanics*, Vol. 229, July 1991, pp. 269-289.doi:10.1017/S0022112091003026

[7] Ortega, J. M., Bristol, R. L. and Savas, O. "Wake Alleviation Properties of Triangular-Flapped Wings." *AIAA Journal*, 40, No. 4, 2002, pp. 709–721.doi:10.2514/2.17.03

[8] Elsenaar, B. "Wake Vortex Research Needs for 'Improved Wake Vortex Separation Ruling' and 'Reduced Wake Signatures'." *WakeNet2-Europe, Pt. 1: Summary and Recommendations*, Amsterdam, Netherlands, 11 April 2006, pp. 1–49.

[9] Babie, B. M., and Nelson, R. C. "Flow Visualization Study of Far Field Wake Vortex Interactions." *11th International Symposium on Flow Visualization*, Univ. of Notre Dame, Notre Dame, IN, August 2004, pp. 1-10.

[10] Matalanis, C. G. and Eaton, J. K. "Wake Vortex Alleviation Using Rapidly Actuated Segmented Gurney Flaps." *The Stanford Thermal and Fluid Sciences Affiliates and the Office of Naval Research*, Stanford University, Stanford, 2007.

[11] Rossow, V. J. "Prospects for Alleviation of Hazard Posed by Lift-Generated Wakes." *Proceedings of the Aircraft Wake Vortices Conference*, Federal Aviation Administration DOT/FAA/SD-92/1.1, Washington, D.C., Oct. 1991, pp. 22-40.

[12] Fabre, D., Jacquin, L., and Loof, A. "Optimal Perturbations in a Four-Vortex Aircraft Wake in Counter-Rotating Configuration." *Journal of Fluid Mechanics*, Vol. 451, 2002, pp. 319-328.

[13] Durston, D. A., Walker, S. M., Driver, D. M., Smith, S. C. and Savas, O. "Wake-Vortex Alleviation Flowfield Studies." *Journal of Aircraft*, Vol. 47, No. 4, 2005, pp. 894-907.

[14] Savas, O. "Experimental Investigations on Wake Vortices and their Alleviation." *Comptes Rendus Physique, Academie des Sciences*, Paris, 6(4-5), 2005, pp. 415-429.

[15] Corsiglia, V. R., Jacobsen, R. A. and Chigier, N. "An Experimental Investigation of Trailing Vortices behind a Wing with a Vortex Dissipater." *Aircraft wake turbulence and its detection*, Plenum, New York, 1971, pp. 229-242.

[16] Patterson, J. C. "Vortex Attenuation Obtained in the Langley Vortex Research Facility." *Journal of Aircraft,* Vol. 12, No. 9, 1975, pp. 745-749.

[17] Breitsamter, C. "Wake Vortex Characteristics of Transport Aircraft." *Progress in Aerospace Sciences*, Vol. 47, No. 2, 2011, pp. 89-134.doi:10.1016/j.paerosci.2010.09.002

[18] Lee, T. and Pereira, J. "Modification of Static-Wing Tip Vortex via a Slender Half-Delta Wing." *Journal of Fluids and Structures*, Vol. 43, Nov. 2013, pp. 1-14. doi:10.1016/j.jfluidstructs.2013.08.004

[19] Altaf, A., Thong, T. B., Omar, A. A. and Asrar, W. "Influence of a Reverse Delta Type Add-on Device on Wake Vortex Alleviation." *AIAA Journal*, Vol. 54, No. 2, 2016, pp. 625-636. Doi: 10.2514/1.J054436.

[20] Altaf, A., Thong, T. B., Ali Omar, A., and Asrar, W. "Impact of a Reverse Delta Type Add-on Device on the Flap-tip Vortex of a Wing." *International Journal of Aviation, Aeronautics, and Aerospace*, Vol. 3, No. 3, Art. 12, 2016, pp. 1-26.

[21] Zhang H. J., Zhou, Y. and Whitelaw, J. H. "Near Field Wing-Tip Vortices and Exponential Vortex Solution." *Journal of Aircraft*, Vol. 43, No. 2, 2006, pp. 445-449. doi: 10.2514/1.15938

[22] "Wake Turbulence: An Obstacle to Increased Air Traffic Capacity." *National Research Council of the National Academies*, The National Academies Press, Washington D.C, 2008.

[23] Figliola, R. S., and Beasley, D. E. *Theory and Design for Mechanical Measurements.* 2nd edition, Wiley, Singapore, 1995, pp. 161-198.

[24] Prandtl, L. *Tragflugeltheorie, II Mitteilung*. Nachrichten der Gesellschaft der Wisseneschaften zu Gottingen, Math, Physik K1, 1919, pp. 107–137.
[25] Reynolds, O. "On the Resistance Encountered by Vortex Rings and Relation between the Vortex Rings and the Streamlines of a Disk." *Nature*, Vol. 14, September 1876, pp. 477-479.
[26] Maxworthy, T. "The Structure and Stability of Vortex Rings." *Journal of Fluid Mechanics*, Vol. 51, No. 1, Jan. 1972, pp. 15-32.doi:10.1017/S0022112072001041
[27] Saffman, P. G. "The Number of Waves on Unstable Vortex Rings." *Journal of Fluid Mechanics*, Vol. 84, No. 4, Feb. 1978, pp. 625-639. doi:10.1017/S0022112078000385
[28] Anderson, J. D. *Fundamentals of Aerodynamics.* 3rd edition, McGraw Hill, Singapore, 2001, pp. 215.
[29] Dobrev, I., Maalouf, B., Troldborg, N., and Massouh, F. "Investigation of the Wind Turbine Vortex Structure." *14th International Symposium on Applications of Laser Techniques to Fluid Mechanics*, Lisbon, July 2008, pp. 1-10.
[30] Rossow, V. J. "Effect of Wing Fins on Lift-Generated Wakes." *Journal of Aircraft*, Vol. 15, No. 3, 1978, pp. 160-167. doi:10.2514/3.58335
[31] Croom, D. R. & Holbrook, G. T. "Low Speed Wind Tunnel Investigation of Wing Fins as Trailing Vortex Alleviation Devices on a Transport Airplane Model." NASA TP-1453, 1979.
[32] Ozger, E., Schell, I., & Jacob, D. "On the Structure and Attenuation of an Aircraft Wake." *Journal of Aircraft*, Vol. 38, No. 5, 2001, pp. 878–887. doi:10.2514/2.2847